









Seasonal and drought-related changes in leaf area profiles depend on height and light environment in an Amazon forest

Marielle N. Smith^{1,2} , Scott C. Stark¹, Tyeeen C. Taylor² , Mauricio L. Ferreira³ , Eronaldo de Oliveira⁴, Natalia Restrepo-Coupe^{2,5} , Shuli Chen², Tara Woodcock², Darlison Bentes dos Santos⁶, Luciana F. Alves⁷ , Michela Figueira⁴, Plinio B. de Camargo³, Raimundo C. de Oliveira⁸ , Luiz E. O. C. Aragão^{9,10}, Donald A. Falk^{11,12} , Sean M. McMahon¹³ , Travis E. Huxman¹⁴ and Scott R. Saleska²

¹Department of Forestry, Michigan State University, East Lansing, MI 48824, USA; ²Ecology & Evolutionary Biology, University of Arizona, Tucson, AZ 85721, USA; ³Centro de Energia Nuclear na Agricultura (CENA), Universidade de São Paulo, Piracicaba, SP 13416-000, Brazil; ⁴Universidade Federal do Oeste do Pará (UFOPA), CEP 68040-255, Santarém, PA, Brazil;

⁵School of Life Sciences, University of Technology Sydney, Sydney, NSW 2007, Australia; ⁶Centro Universitário Luterano de Santarém (CEULS/ULBRA), CEP 68.025-000, Santarém, PA, Brazil; ⁷Center for Tropical Research, Institute of the Environment and Sustainability, UCLA, Los Angeles, CA 90095, USA; ⁸Embrapa Amazônia Oriental, 68035-110, Santarém, PA, Brazil;

⁹Instituto Nacional de Pesquisas Espaciais, 12227-010, São José dos Campos, SP, Brazil; ¹⁰College of Life and Environmental Sciences, University of Exeter, Exeter, EX4 4RJ, UK; ¹¹School of Natural Resources and the Environment, University of Arizona, Tucson, AZ 85721, USA; ¹²Laboratory of Tree-Ring Research, University of Arizona, Tucson, AZ 85721, USA; ¹³Smithsonian Institution Forest Global Earth Observatory, Smithsonian Environmental Research Center, Edgewater, MD 21037, USA; ¹⁴Ecology and Evolutionary Biology and Center for Environmental Biology, University of California, Irvine, CA 92629, USA

Summary

Author for correspondence:

Marielle N. Smith

Tel: +1 520 3146346

Email: mariellenatashsmith@gmail.com

Received: 25 September 2018

Accepted: 4 January 2019

New Phytologist (2019) 222: 1284–1297

doi: 10.1111/nph.15726

Key words: Amazon forest, climate change, El Niño drought, forest canopy structure, leaf area, LiDAR remote sensing, phenology.

- Seasonal dynamics in the vertical distribution of leaf area index (LAI) may impact the seasonality of forest productivity in Amazonian forests. However, until recently, fine-scale observations critical to revealing ecological mechanisms underlying these changes have been lacking.
- To investigate fine-scale variation in leaf area with seasonality and drought we conducted monthly ground-based LiDAR surveys over 4 yr at an Amazon forest site. We analysed temporal changes in vertically structured LAI along axes of both canopy height and light environments.
- Upper canopy LAI increased during the dry season, whereas lower canopy LAI decreased. The low canopy decrease was driven by highly illuminated leaves of smaller trees in gaps. By contrast, understory LAI increased concurrently with the upper canopy. Hence, tree phenological strategies were stratified by height and light environments. Trends were amplified during a 2015–2016 severe El Niño drought.
- Leaf area low in the canopy exhibited behaviour consistent with water limitation. Leaf loss from short trees in high light during drought may be associated with strategies to tolerate limited access to deep soil water and stressful leaf environments. Vertically and environmentally structured phenological processes suggest a critical role of canopy structural heterogeneity in seasonal changes in Amazon ecosystem function.

Introduction

As the largest intact tropical rainforest in the world, the Amazon plays a critical role in global climate processes and biodiversity maintenance (Dirzo & Raven, 2003; Malhi *et al.*, 2008). Changes to Amazonian forests could affect local, regional, and global atmospheric circulation, resulting in altered precipitation patterns (Gedney & Valdes, 2000; Werth & Avissar, 2002; Spracklen *et al.*, 2012; Garcia *et al.*, 2016) and atmospheric carbon content (Pan *et al.*, 2011). As such, it is critical to understand the controls on Amazon forest productivity, which is highly to moderately seasonal, ranging from zero to five dry season months (Restrepo-Coupe *et al.*, 2013). Ecosystem function is influenced

further by interannual climate variation, particularly droughts associated with El Niño Southern Oscillation and other factors, which are expected to increase in frequency and severity with climate change (Malhi *et al.*, 2008; Chadwick *et al.*, 2015; Duffy *et al.*, 2015). The patterns and mechanisms of Amazon forest response to this variation, however, remain incompletely characterised and poorly understood (Sitch *et al.*, 2008; Malhi *et al.*, 2009).

Vegetation model predictions for dry season photosynthesis differ from ecosystem-level field observations (Restrepo-Coupe *et al.*, 2017). Whereas eddy flux observations at central Amazon sites show increases in gross primary productivity (GPP) during the dry season (Saleska *et al.*, 2003; Goulden *et al.*,

2004; Hutrya *et al.*, 2007; Restrepo-Coupe *et al.*, 2013), consistent with satellite metrics of canopy function (enhanced vegetation index, EVI; Huete *et al.*, 2006; Saleska *et al.*, 2007; but see debate: Morton *et al.*, 2014; Saleska *et al.*, 2016; Wu *et al.*, 2016), land surface models simulate dry season productivity declines (Restrepo-Coupe *et al.*, 2017). This contradiction indicates an incomplete understanding of tropical forest phenology, which limits prediction of the impacts of expected increases in the length and intensity of dry seasons with climate change (Duffy *et al.*, 2015).

Likely mechanisms of GPP seasonality include seasonal environmental changes and phenological changes in vegetation function (i.e. changes in canopy biophysical properties) (Albert *et al.*, 2018). GPP may respond directly to changes in radiation and precipitation (Wright & van Schaik, 1994; Guan *et al.*, 2015; Wagner *et al.*, 2017) (climatic environments, H_{env}), or be driven by an evolved 'phenological clock', whereby phenology strictly follows annually consistent environmental cues (e.g. daylength or solar zenith angle, SZA; H_{clock}) (Borchert, 1980; van Schaik *et al.*, 1993; Reich, 1995; Rivera *et al.*, 2002). Alternatively, or additionally, GPP seasonality may be due to seasonal changes in vegetation structure and function, especially leaf quantity (leaf area index, LAI) and leaf quality (photosynthetic capacity, P_c), respectively (Albert *et al.*, 2018). Among these, leaf quality – a function of leaf age demography and leaf age-dependent physiology – has recently been found to contribute to seasonal patterns of ecosystem fluxes (Wu *et al.*, 2016; Albert *et al.*, 2018). By contrast, leaf quantity (total LAI) exhibits low seasonal variation and appears to have relatively little impact on photosynthetic seasonality (Wu *et al.*, 2016). However, analyses of total LAI may mask important seasonal shifts in the vertical distribution of leaf area across canopy microenvironments, which could significantly alter forest function. Indeed, a recent analysis of satellite light detection and ranging (LiDAR) across the Amazon basin found strong, anticorrelated seasonality of lower and upper canopy leaf area, potentially implicating light limitation imposed by canopy self-shading in GPP seasonality (H_{light} ; Tang & Dubayah, 2017). Alternatively, such a pattern may arise from biological factors associated with vegetation height (e.g. functional groups, hydraulics, rooting depths) (H_{height}).

Although effective for macroscale phenological patterns, analysis of large footprint LiDAR data (c. 65 m in diameter; Tang & Dubayah, 2017) may conceal important fine-scale heterogeneity. Light environments are highly variable in the lower canopy, encompassing light gaps and deep shade (understory) (Chazdon & Fetcher, 1984; Smith *et al.*, 1992), but tend to be more consistent (high light) in the upper canopy. Lower canopy trees span a wide functional spectrum from light-demanding to shade-tolerant (Wright *et al.*, 2010). The high diversity of functional strategies and microenvironments may promote a variety of distinct phenological and drought responses among lower canopy trees, which could meaningfully influence GPP seasonality while remaining undetected by aggregate and large-scale forest metrics.

To improve our understanding of the vertical dynamics of tropical evergreen forest canopies, we used monthly ground-based LiDAR measurements to investigate seasonal and drought

responses of leaf area along gradients of canopy height and light environment at an Amazonian site. Measurements were collected over 4 yr, including an El Niño-related drought event (2015–2016). The high vertical and horizontal resolution of our observations (2 m) can uniquely distinguish the responses of different canopy layers to distinct light environments. In addition, we compare the seasonality of LiDAR-derived leaf area profiles with the seasonality of the satellite-derived EVI metric of canopy function. We test the following hypotheses:

(1) Biophysical heterogeneity through the canopy gives rise to vertically dynamic LAI shifts in response to seasonal environmental change. Specifically, we test the effects of biological factors (H_{height} and H_{clock}), climatic environments (H_{env}), and within-canopy environments (H_{light}).

(2) The response of canopy structure to drought will be an amplification of the response to seasonal water deficit (drought intensification hypothesis, H_{drought} ; Huete *et al.*, 2006; Saleska *et al.*, 2007).

(3) Vertically structured leaf area dynamics will explain dry season 'greening' interpreted from satellite-derived vegetation indices (Huete *et al.*, 2006; Saleska *et al.*, 2016; Wu *et al.*, 2016). Specifically, we predict that reflectance indices will correlate most strongly with upper canopy LAI, since satellites primarily detect changes in the upper canopy (H_{evi} ; Bradley *et al.*, 2011; Biudes *et al.*, 2014).

Materials and Methods

Study site

The Tapajós National Forest (TNF) K67 site (2°51'S, 54°58'W) is a *terra firme* tropical moist forest, with 1993 mm of mean annual precipitation, an average temperature of 25°C, and a 5-month dry season between July and November (months with < 100 mm rainfall; Restrepo-Coupe *et al.*, 2013), which is within the upper 30th percentile of dry season length within the Amazon (Saleska *et al.*, 2003). Owing to its combination of wet forest structure and strong dry season, this forest has been considered a likely bellwether for climate change responses (Saleska *et al.*, 2003).

LiDAR data collections

Ground-based LiDAR surveys were made using Riegl LD90-3100VHS-FLP systems (Riegl Laser Measurement Systems, Horn, Austria; Supporting Information Notes S1; Fig. S1). Sampling was conducted at a constant pace along four 1 km survey transects (4 km in total). Pulse return data were used to estimate leaf area density (LAD, m² m⁻³) throughout a vertical 'sampling plane' in the canopy (Parker *et al.*, 2004). Surveys were conducted during three periods: January to December 2010, August to December 2012, and November 2015 to June 2017, for a total of 41 surveys, encompassing three non-El Niño years or partial years (January to December 2010, August to December 2012, and July 2016 to June 2017) and one El Niño drought year (November 2015 to June 2016). Surveys were made monthly

except for in 2012, when they were bimonthly. Survey transects corresponded with central axes of forest inventory plots, where litterfall collection baskets were located (see the Methods section 'Leaf litterfall and flush').

Deriving LAI and leaf area profiles from LiDAR data

We divided point returns volumetrically, with 2 m horizontal (along transects) and 1 m vertical increments (with 1 m the approximate horizontal laser pulse width). We then applied the MacArthur–Horn transformation (MacArthur & Horn, 1969) to pulse transmission rates in each voxel to estimate LAD following Stark *et al.* (2012), which accounts for occluded material based on return density. Transects were divided into 16 plots (each 250 m) for estimation of mean and standard error of leaf area profiles, and, summing vertically, LAI values. We adjusted the annual mean LAI across non-El Niño years to a published site mean of 5.7 (Stark *et al.*, 2012) by setting the extinction constant k to 0.75 to make our results comparable to other studies. We assessed potential sampling sensitivities to rule out artefactual results (Notes S2; Figs S2, S3) and quantified sensor-based error (Notes S3; Fig. S4).

We analysed leaf area seasonality with respect to absolute distance from the ground ('absolute height arrangement') to test H_{height} , and with respect to distance from the local canopy surface ('illumination environment arrangement'; Fig. 1) to categorise leaf area by light availability and to help test H_{light} (for dataset, see Notes S4). The absolute height arrangement separated the canopy into lower (0–15 m) and upper (> 15 m) levels to reveal contrasting dynamics. The 15 m cutoff is approximately the height at which there was a direction reversal in LAD change (detailed in the Results section). The illumination environment arrangement divided the canopy into four layers of approximately equal LAI with respect to *depth from the canopy surface*, corresponding to depths of 1–2 m (canopy surface layer), 3–7 m, 8–15 m, and > 15 m (deepest or understory layer). For the analyses to assess relationships between canopy LAI layers, reflectance, and environmental variables (see the Methods section 'Canopy LAI layer, reflectance, and orbitally determined radiation relationships'), we further divided the canopy surface layer into canopy heights ≤ 20 m and > 20 m (henceforth referred to as 'lower surface' and 'upper surface' layers, respectively), and for the deepest understory layer we considered only vegetation ≤ 20 m (referred to as 'understory'). The 20 m cut-off is the height approximating a direction reversal in LAD changes for the illumination environment arrangement. We scaled LAI for the whole canopy and individual layers by annual means ('normalised LAI') in order to analyse detrended patterns ('relative seasonality') independently of interannual variation in LAI (Fig. S5).

To analyse regular seasonal differences in leaf area profiles, and to test H_{drought} by comparing these with El Niño patterns, we followed Restrepo-Coupe *et al.* (2013) to define start dates of the dry (1 July) and wet (1 December) seasons and seasonal mid-points (15 September and 17 March, respectively). LiDAR surveys closest to the target dates were selected, adjusting if needed

to ensure at least 1 month between the dates of the LiDAR surveys used to calculate profile differences for half-season intervals.

All analyses were conducted using R software (R Core Team, 2016).

Leaf litterfall and flush

Monthly litterfall collections concurrent with LiDAR survey years were available from July 2012 to June 2013 and July 2015 to July 2016. Nonoverlapping bimonthly litterfall data were also available July 2000 to June 2005 (Rice *et al.*, 2004); average monthly values from this long-term dataset were used to estimate leaf flush values for 2010. Collections were made from 40 (2000–2005), 64 (2012–2013), or 78 baskets (2015–2016) located along site survey transects. Dried leaf litterfall weights were converted to leaf area ($\text{m}^2 \text{m}^{-2}$) multiplying by specific leaf area ($0.0032 \text{ m}^2 \text{g C}^{-1}$; Domingues *et al.*, 2005). Leaf flush (area of newly produced leaves, $\text{m}^2 \text{m}^{-2}$) was estimated as the sum of change in LiDAR-derived LAI (dLAI, $\text{m}^2 \text{m}^{-2}$) and leaf litterfall measurements ($\text{m}^2 \text{m}^{-2}$) between LiDAR surveys (Fig. S6).

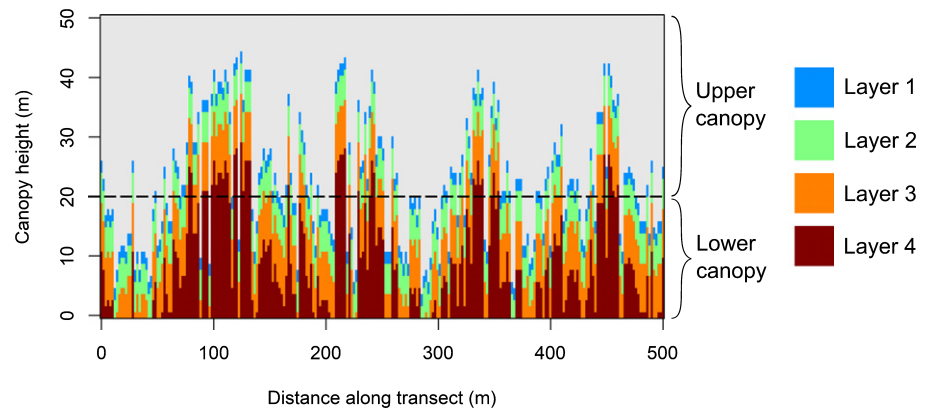
Assessing differences between seasonal ranges: LAI, leaf litterfall, and leaf flush

We calculated annual ranges (the difference between maximum and minimum annual values) of LAI (total, lower, and upper), litterfall, and leaf flush (Table S1). To compare dynamics at the survey scale (full spatial extent of sampling), we generated bootstrapped means and 95% confidence intervals (CIs) for normalised ranges (the annual percentage change, calculated as the annual range divided by the mean annual value and multiplied by 100) across non-El Niño years and all years. Means and CIs were generated from 1000 bootstrap samples, each comprising a random assembly of a year's worth of data; the year from which each monthly value originated was randomly assigned (month identity was never reassigned due to seasonal pattern). We report but did not bootstrap CIs for nonnormalised ranges because interannual variations in absolute values would lead to unrealistic resampled ranges. Mean annual normalised ranges of canopy layer LAI, litterfall, and leaf flush (calculated across all years) were considered significantly different if their respective bootstrap 95% CIs were nonoverlapping. El Niño normalised ranges were considered significantly different from baseline years if they fell outside the baseline bootstrapped 95% CIs. Mean annual ranges and 95% CIs at the plot level (nonnormalised and normalised) were calculated directly from all plots across all years without bootstrapping ($n = 62$).

EVI and near-infrared values

To test H_{evi} we employed EVI and near-infrared (NIR) data from the Moderate Resolution Imaging Spectroradiometer (MODIS) using the Multi-Angle Implementation of Atmospheric Correction (MAIAC) algorithm, which included strict atmosphere, aerosol, and cloud correction and bidirectional reflectance distribution function correction (Lyapustin *et al.*, 2012). By largely

Fig. 1 The canopy illumination environment arrangement in which LiDAR data were separated into four layers of varying light availabilities, defined by different distances away from the local canopy surface. Layers comprise leaf area density ($\text{m}^2 \text{m}^{-3}$) values within voxels 1–2 m (layer 1, the canopy surface layer, blue), 3–7 m (layer 2, green), 8–15 m (layer 3, orange), and > 15 m (layer 4, the deepest or understory layer, red) away from the top of the canopy. The black dashed line at 20 m shows the division of canopy data into upper and lower levels.



removing such artefact effects, MAIAC data can reveal more realistic seasonal vegetation greenness in Amazon forests than standard MODIS EVI/NIR observations can (Wu *et al.*, 2018). Annual seasonal patterns were derived from monthly mean values over a 12 yr period (2000–2012) for a $3 \times 3 \text{ km}^2$ tile centred on the K67 site.

Environmental variables

We obtained monthly precipitation data from the Tropical Rainfall Measuring Mission (3B43-v7; TRMM, 2011), SZA data from NOAA ESRL Global Monitoring Division (2018) and daylength values for the closest city (Santarém, 36 miles away; Time and Date AS, 2018). We also matched mean monthly site-level above-canopy incident net radiation and vapour pressure deficit (VPD) measured at the K67 eddy flux tower (updated version of dataset by Restrepo-Coupe *et al.*, 2013) for the previous month, to each LiDAR survey date. VPD was calculated from above-canopy sensors measuring H_2O concentration and temperature at 57.8 m above ground (*c.* 23 m from the canopy surface).

Canopy LAI layer, reflectance, and orbitally determined radiation relationships

We explored a correlation matrix of reflectance metrics (EVI and NIR), leaf area components (total LAI and LAI layers normalised by annual means), and environmental drivers (daylength and SZA), restricting analysis to non-El Niño years. Whereas daylength and SZA values corresponded to the full LiDAR leaf area timeseries, EVI and NIR values were restricted to the 10-yr averaged pattern of seasonality. Since new leaves mature in 3–5 months (Wu *et al.*, 2016; Albert *et al.*, 2018), we considered possible time lags in correlation. Trying all 1–4 month lags, we report the highest R^2 relationships significant at $P < 0.01$. Lags where R^2 values increased by < 0.10 are not reported.

Multiple regression analysis to identify drivers of phenology

To test hypotheses of phenological drivers, we conducted a series of multiple regression analyses on the most distinct combination of layers from the absolute height arrangement and canopy

illumination arrangement. For each selected LAI component – total LAI, upper and lower LAI, and lower surface, upper surface, and understory LAI – we tested all possible combinations of environmental predictor variables, including climatic environmental variables (VPD, radiation, and precipitation) and those determined by Earth's orbit (SZA or daylength, and their quadratics). For lower LAI components, upper canopy LAI was also included as a predictor. After merging available data, 36 out of 41 total surveys were included for analysis. We present the best model for each LAI component (selected via the lowest Akaike information criterion, AIC) and the relative importance of each predictor variable (calculated as the sum of the relative evidence weights/probabilities across all models in which the variable was present; R package GLMULTI; Calcagno & da Mazancourt, 2010). If climatic environmental variables are important, we find support for H_{env} ; Earth-orbit variable importance would support H_{clock} . A light limitation effect (H_{light}) may be supported if increasing upper LAI predicts decreasing lower LAI (but see the Discussion section).

Results

Seasonal patterns of total LAI, leaf litterfall, and leaf flush

LAI increased throughout most of the dry season and decreased at the onset of the wet season (Figs 2, S5). Across all years, the annual range of LAI varied between 0.10 and $0.18 \text{ m}^2 \text{m}^{-2}$ and the mean annual normalised range was 2.58% (CI: 1.57–3.48; Table S1). The plot-level mean annual range ($0.50 \text{ m}^2 \text{m}^{-2}$; CI: 0.46–0.55) and normalised range (8.87%; CI: 8.10–9.65) were higher than the survey-level. Leaf litterfall peaked during the dry season and reached minimum values during the wet season. Estimated leaf flush followed a similar seasonal cycle to leaf litterfall. Mean annual normalised ranges of leaf litter (141.23%; CI: 92.92–177.34) and leaf flush (204.26%; CI: 136.94–255.77) were significantly higher than LAI (95% CIs did not overlap).

Supporting H_{drought} , the highest ranges of leaf litterfall, leaf flush, and LAI were all recorded in the El Niño year (0.34, 0.43, and $0.18 \text{ m}^2 \text{m}^{-2}$, respectively), although the mean annual normalised ranges were only significantly different for total LAI

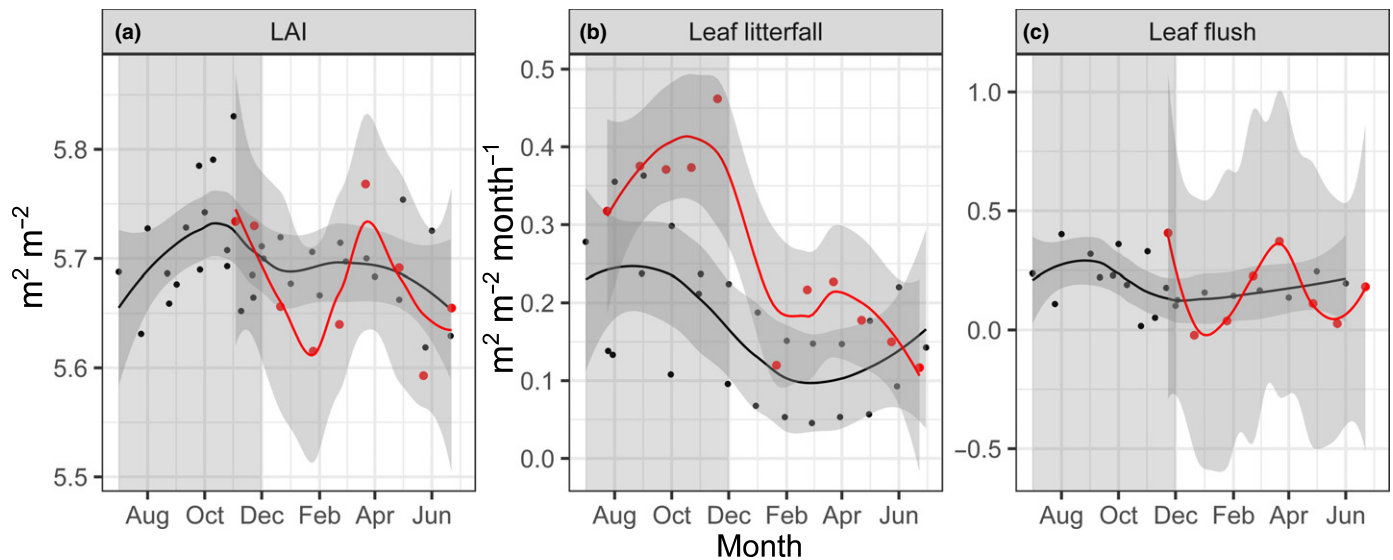


Fig. 2 Seasonal values of (a) leaf area index (LAI), (b) leaf litterfall, and (c) estimated leaf flush, for non-El Niño years (2010, 2012 and 2016–2017, black) and a 2015–2016 severe El Niño drought (red). Lines are loess fits with a span value of 0.7; grey shading displays 95% confidence intervals (CIs) on this fit. Grey boxes (July–December) indicate dry season months. Leaf flush was calculated as the sum of change in LiDAR-derived LAI (dLAI, and leaf litterfall; litterfall rates were interpolated according to LiDAR survey dates. Leaf litterfall and flush exhibited significantly higher seasonal variation than total LAI (based on bootstrapped mean annual normalised ranges and 95% CIs across all years; litterfall: 141.23%, CI 92.92–177.34; flush: 204.26%, CI 136.94–255.77; LAI: 2.58%, CI 1.57–3.48). Normalised range for total LAI during the El Niño year (3.09%) exceeded that of non-El Niño years (2.29%; CI: 1.50–3.01), but normalised range for litterfall was not significantly different. Statistical difference for leaf flush could not be assessed due to small sample size (see the Results section and Supporting Information Table S1).

(non-El Niño: 2.29%; CI: 1.50–3.01; El Niño: 3.09%). Two of the lowest LAI values across the whole timeseries were recorded during the El Niño year (in January 2015 and May 2016).

Seasonal patterns of LAI in the lower and upper canopy strata

Canopy strata exhibited significantly greater seasonal variation than total LAI. Mean annual normalised ranges were 7.02% (CI: 3.85–9.89) and 11.19% (CI: 6.56–16.56) for lower and upper canopy layers, respectively, vs 2.58% (CI: 1.57–3.48) for total LAI. When considering variation in 250 m plots, we find higher values, with mean annual normalised ranges of 11.97% (CI: 10.89–13.05), 21.63% (CI: 19.28–23.97), and 8.87% (CI: 8.10–9.65) for lower, upper, and total LAI, respectively. Considering normalised values, lower canopy LAI exhibited a bimodal seasonality, increasing during the first halves of the dry and wet seasons and decreasing in the second halves of both seasons (Fig. 3). The upper canopy showed the opposite seasonal pattern; accordingly, the upper and lower canopies were significantly anticorrelated ($R^2 = 0.57$, $P < 0.0001$ across all non-El Niño years; $R^2 = 0.43$ – 0.84 , $P < 0.05$ within years, Fig. S7). Note that this strong significant anticorrelation effectively increases confidence in the annual changes within layers.

Consistent with H_{drought} , seasonal ranges increased during the El Niño drought: nonnormalised ranges of the lower and upper canopy levels were 50% and 30% higher, respectively, than baseline years. However, the differences were significant only for the normalised range of the lower canopy (non-El Niño: 6.05%; CI: 3.61–8.71; El Niño: 9.89%). The impact of El Niño was most

evident when considering the dynamics of the whole vertical profile (see the Results section ‘Seasonal changes in leaf area profiles: absolute height arrangement’). Plot-level trends were highly consistent at the peak of El Niño (November–December 2015), with the majority of plots showing an increase in leaf area in the upper canopy and a decrease in the lower canopy (Fig. S8). Layer leaf area dynamics appeared to fall within the range of previous years by April 2016 (mid wet season) after the drought (Fig. 3).

Seasonal changes in leaf area profiles: absolute height arrangement

Vertical profiles of seasonal changes in LAD show how opposing shifts across canopy heights can balance to a seasonally neutral total LAI (Fig. 4). Supporting H_{height} , leaf area was lost from the lower canopy and gained in the upper canopy from the middle to the end of the dry season (Fig. 4c). Immediately following, in the start to mid wet season, these trends reversed (Fig. 4d). Throughout the study, leaf area profile dynamics alternated between these two different phases (upper canopy increase concurrent with lower canopy decrease and vice versa) each half-season period. The direction of LAD change reversed at $c.$ 15 m within each period. Trends were consistent across years but more pronounced during the 2015–2016 El Niño year (Figs 4, S9). LAD changes in the lower canopy, the stratum of greatest leaf area in this forest (Stark *et al.*, 2012), dominated the profile dynamics in terms of absolute LAI change (Fig. 4). Profile changes during the El Niño year were greatest from the middle to the end of the dry season. By the end of the wet season they appeared similar to prior years.

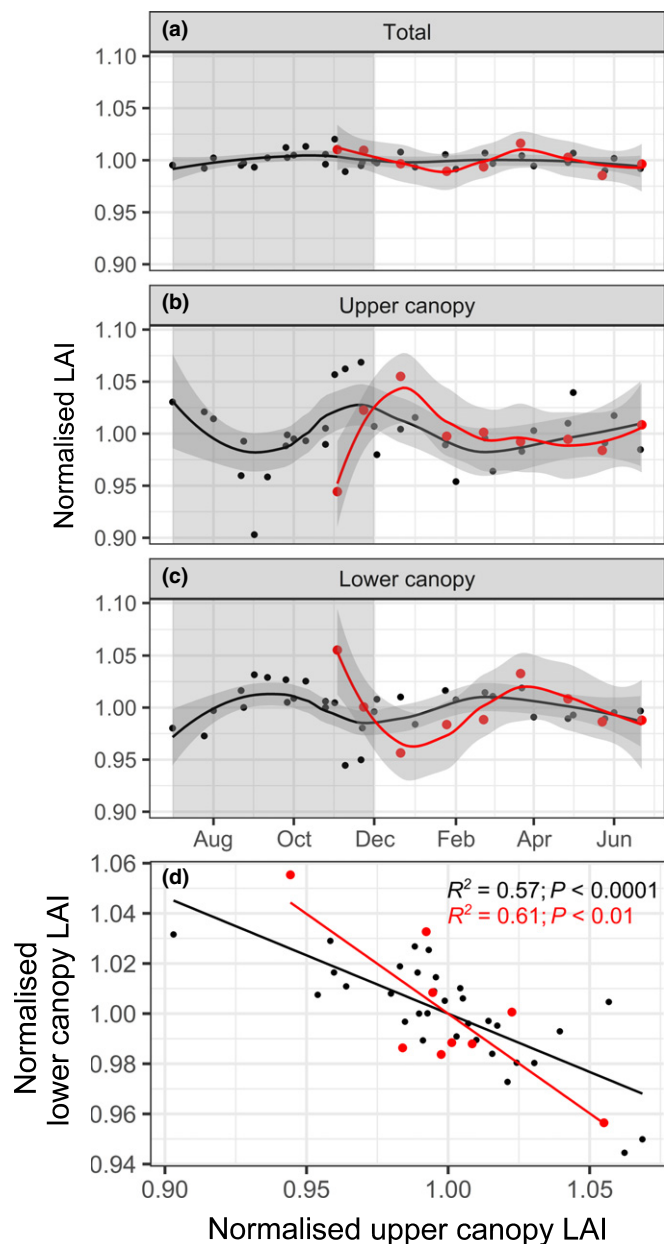


Fig. 3 Seasonality of (a) total leaf area index (LAI), (b) upper (> 15 m) and (c) lower (≤ 15 m) canopy layers, as defined by distance from the ground, and (d) the relationship between lower and upper canopy LAI. Black lines show data for non-El Niño years (2010, 2012, and 2016–2017), and red lines show values for an El Niño year (2015–2016). LAI values are scaled to the mean for each year ('normalised LAI'). In (a–c), lines are loess fits with a span value of 0.7, and shading displays 95% confidence intervals on this fit. Grey boxes indicate dry season months. Upper and lower canopy LAI exhibited significantly higher seasonal variation than total LAI (based on bootstrapped mean annual normalised ranges and 95% CIs across all years; total LAI: 2.58%, CI 1.57–3.48; upper LAI: 11.19%, CI 6.56–16.56; lower LAI: 7.02%, CI 3.85–9.89). Normalised ranges for total and lower canopy LAI during the El Niño year (3.09% and 9.89%, respectively) exceeded normalised ranges during non-El Niño years (2.29%, CI 1.50–3.01 and 6.05%, and CI 3.61–8.71, respectively), but normalised range for upper canopy LAI was not significantly different (see the Results section and Supporting Information Table S1).

Seasonal changes in canopy depth layers: illumination environment arrangement

Dividing the canopy into four layers (Fig. 1) by depth (illumination environment) categories revealed that much of the lower canopy constitutes surface leaves of smaller trees (Fig. 5a, layers 1–2), rather than shaded understory vegetation (Fig. 5a, layers 3–4). Analysis by depth layer reveals that the decrease in the lower canopy (< 20 m) leaf area from the mid to the end of the dry season (Fig. 4c) is actually driven by losses in the canopy surface (Fig. 5c). The seasonal dynamics of depth layers within the upper canopy were generally consistent within each period (Fig. S10). Below 20 m, however, canopy layers exhibited a greater variety of responses; in particular, the deepest understory layer (layer 4) typically opposed the dynamics of the lower canopy surface layers (layers 1 and 2). In contrast to expectation by light limitation (H_{light}) of the upper canopy on subcanopy leaves, understory leaf area shifts did not oppose the upper canopy, but rather matched upper canopy trends while opposing trends in the lower surface (Fig. 6). Strong layer anticorrelations in decreasing order were understory vs lower surface, lower surface vs upper canopy, and lower vs upper (height-defined) ($R^2 = 0.73$ – 0.52), whereas understory and upper canopy layers were positively correlated ($R^2 = 0.65$, $P < 0.0001$; Table S2; Fig. S11). The upper canopy surface layer was not significantly correlated with other layers, displaying a contrasting unimodal seasonal pattern (Fig. 6). Illumination environment layer trends were, again, enhanced relative to baseline years during the 2015–2016 El Niño drought, especially in the lower canopy (support for H_{drought} ; Figs S10, S12).

Illumination environment layers also reveal apparent rapid leaf area transitions at the end of the dry–beginning of the wet season. Highlighted by the highly temporally resolved splines in Fig. 6 (thin lines), between November and December, leaf area in the lower surface rebounds from its lowest level to one of its highest, whereas the converse is true for the understory.

Leaf area relationship with canopy reflectance

There was no clear support for H_{evi} . LiDAR-derived leaf area seasonality was related only weakly to the seasonality of satellite-derived canopy reflectance metrics. EVI and NIR were both correlated with the understory layer ($R^2 = 0.25$, $P < 0.01$, and $R^2 = 0.27$, $P < 0.01$, respectively; Table S2). NIR was also correlated with the upper surface layer ($R^2 = 0.18$, $P < 0.01$). These relationships were temporally offset (time-lagged) 2–4 months; there were no significant correlations in the absence of time lags. Reflectance metric seasonality corresponded fairly strongly with SZA and daylength, allowing for time lags ($R^2 = 0.22$ – 0.47 , $P < 0.01$).

Identifying the drivers of phenology

Upper LAI exhibited a U-shaped response to daylength ($R^2 = 0.14$, $P < 0.05$), whereas lower LAI showed the opposite, hump-shaped response ($R^2 = 0.18$, $P < 0.01$; Fig. S13), both

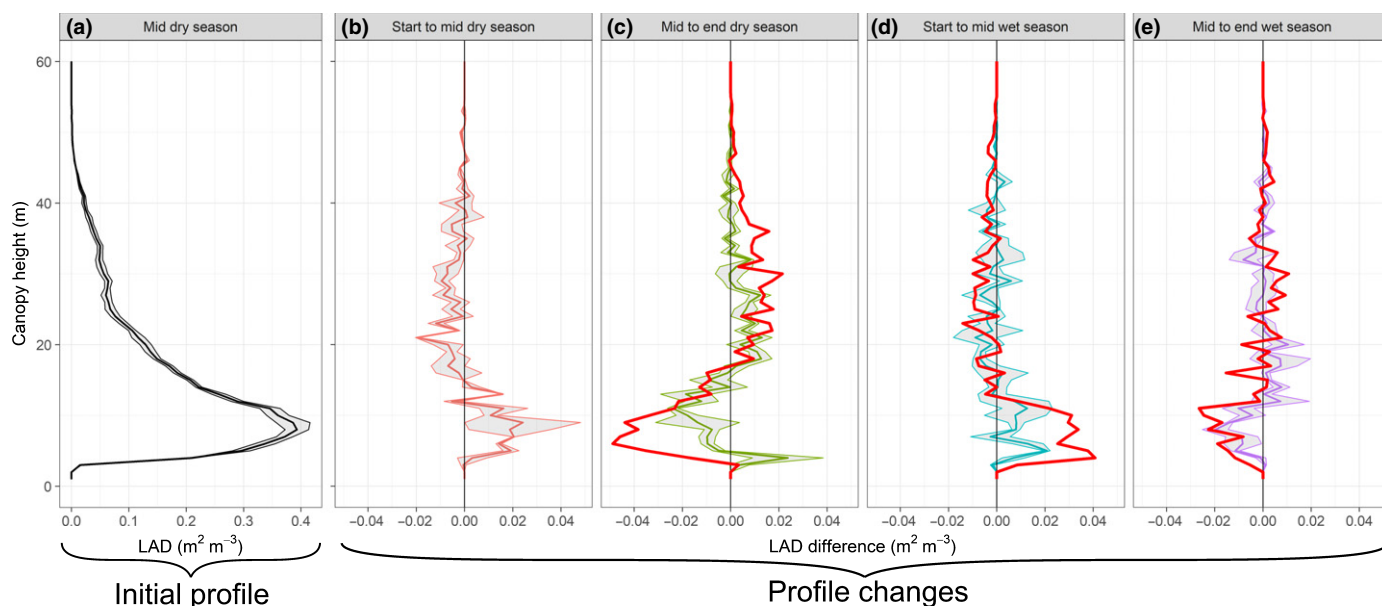


Fig. 4 Seasonal changes in leaf area profiles for non-El Niño years (2010, 2012 and 2016–2017) and a severe El Niño drought year (2015–2016) showing (a) the leaf area density (LAD, $\text{m}^2 \text{m}^{-3}$) vertical profile for the mid dry season (averaged across all years, black) for reference and (b–e) average LAD differences for each half-season period. Red, green, blue and purple lines show mean profiles with standard error for non-El Niño years, and thick red lines show data for the El Niño year. The start and middle of the dry season correspond approximately to July and September–October, respectively, and the start and middle of the wet season approximately to December and March–April, respectively (see the Materials and Methods section).

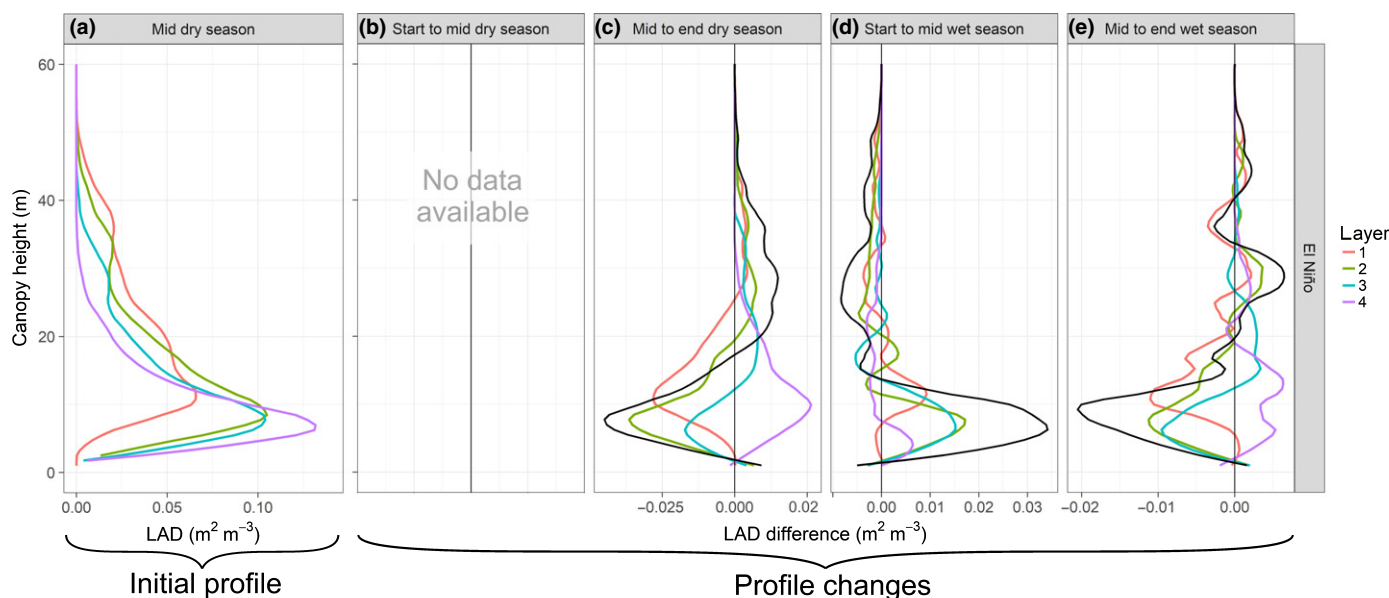


Fig. 5 Seasonal changes in leaf area profiles for the 2015–2016 El Niño drought year separated into canopy depth layers showing (a) the initial mid dry-season leaf area density (LAD, $\text{m}^2 \text{m}^{-3}$) profile and (b–e) LAD differences for each half-season period where data were available. Total profile difference values are shown in black (corresponding to thick red lines in Fig. 4), and coloured lines show profile values for individual canopy layers, based on distance from the local canopy surface. Layer 1 (red): 1–2 m from the top of the canopy (canopy surface); layer 2 (green): 3–7 m; layer 3 (blue): 8–15 m; and layer 4 (purple): > 15 m (deepest or understory layer). Lines are smoothed loess fits with a span of 0.2 to facilitate viewing trends. The start and middle of the dry season correspond approximately to July and September–October, respectively, and the start and middle of the wet season approximately to December and March–April, respectively (see the Materials and Methods section).

providing evidence for H_{clock} . Total LAI exhibited an upward-inflected quadratic relationship with locally measured radiation ($R^2 = 0.24$, $P < 0.01$), providing support for H_{env} . Upper and lower LAI, and lower surface and understory layers, correlated with orbitally determined daylength and SZA, with time lags of

0–3 months ($R^2 = 0.22$ – 0.53 ; Table S2). All layers displayed bimodal trends (Fig. 6) corresponding best with lagged SZA, except the upper canopy surface, which uniquely displayed a unimodal seasonal trend, anticorrelating with daylength 3 months later ($R^2 = 0.39$, $P < 0.0001$).

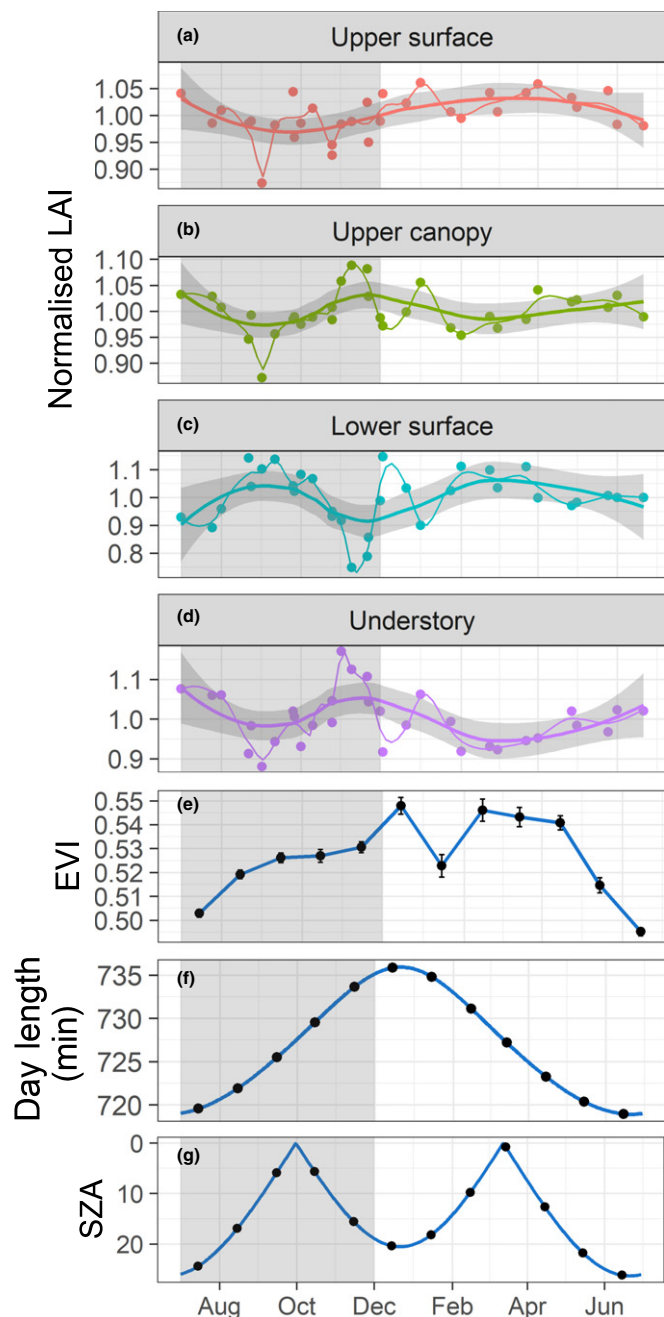


Fig. 6 Seasonality of (a–d) leaf area layers, (e) enhanced vegetation index (EVI), and (f, g) key environmental variables (daylength and solar zenith angle, SZA). Leaf area index (LAI) of the leaf area layers comprises (a) layer 1 > 20 m, (b) all LAI > 20 m, (c) layer 1 ≤ 20 m, and (d) layer 4 ≤ 20 m. Data presented are for non-El Niño years and LAI values are scaled to the mean for each year ('normalised LAI'). Thick smoothed lines on leaf area layer plots are loess fits with a span value of 0.7, with shading to display 95% confidence intervals on this fit; thin smoothed lines are loess fits with a span value of 0.2, to highlight finer timescale dynamics. Grey boxes indicate dry season months. See Supporting Information Table S2 for full results of correlations between LAI layers, environmental variables, and reflectance metrics.

In multiple regression analyses, climatic and orbitally determined environmental variables were important for different leaf area components, offering support for H_{clock} and H_{env} . Radiation

and VPD were the most important variables for predicting total LAI ($R^2 = 0.37$, $P < 0.001$, $\text{AIC} = 91$; Fig. 7; Table S3). For the absolute height arrangement, SZA was the most important predictor of upper canopy LAI ($R^2 = 0.14$, $P < 0.05$, $\text{AIC} = 101$), whereas LAI of the upper canopy, radiation, and VPD were the best predictors of lower canopy LAI ($R^2 = 0.70$, $P < 0.001$, $\text{AIC} = 65$). For the illumination environment arrangement, there were no significant predictors for the upper surface layer; for the lower canopy surface, upper canopy LAI and radiation were the most important predictors ($R^2 = 0.61$, $P < 0.001$, $\text{AIC} = 73$), whereas upper canopy LAI alone was the most important predictor of the deepest understory layer ($R^2 = 0.61$, $P < 0.001$, $\text{AIC} = 72$). Although the upper canopy predicts lower layers, we note that support for light limitation H_{light} is unclear, since lower canopy leaf area decreases occur in the well-illuminated canopy surface, and the understory increases with the upper canopy (Fig. 6; Table S2). We note that a likelihood ratio test found an annual factor ('year') to be nonsignificant for all response variables; hence, we excluded it. We have presented only analyses including SZA since most layers displayed associations with this variable (analysis with the daylength variable is presented in Notes S5 and Table S4).

Synthesis of principal findings

We found that the vertical distribution of leaf area (the LAD profile) is more variable seasonally than total LAI. For example, normalised ranges of upper and lower canopy LAI exceeded the 95% CIs for total LAI (Fig. 3; Table S1). These shifts between the upper and lower levels of profiles were anticorrelated, exhibiting opposing seasonality, which agrees with recent results observed at broader scales with spaceborne LiDAR (Tang & Dubayah, 2017). From the mid to the end of the dry season, leaf area was gained in the upper canopy and lost from the lower canopy, whereas trends reversed at the onset of the wet season (Figs 3, 4).

Investigating phenological drivers across layers of the canopy defined by depth under the canopy surface – reflecting leaf illumination environments – we found surprising patterns consistent with roles of environmental (H_{env}) and biological factors associated with height (H_{height}). Upper canopy LAI phenology tracked SZA, such that leaf area minima approximately corresponded with the orbitally determined biannual apogee of incident solar radiation, supporting a role of a phenological clock (H_{clock}). The seasonality of the well-illuminated surface layer of the lower canopy mirrors that of the upper canopy (i.e. is very similar but of the opposite direction), and the seasonality of the understory layer matches that of the upper canopy (Fig. 6). Height and environment, thus, *both* modulate phenology. Similarly, multiple regression analyses offered some support for a role of climatic environmental variation (H_{env}), particularly for total and lower canopy LAI, where incident radiation and, potentially, VPD were important predictors.

The strength of correlations between SZA or daylength and leaf area layers was consistent across height and depth strata (Table S2), such that the signal of seasonality appeared similar throughout sunlit and shaded canopy layers. Relationships

between the layers themselves, however, were stronger; specifically, the anticorrelations between the lower canopy surface and understory layers, the full upper canopy and the lower canopy surface, and the full upper and lower canopy levels. These relationships explained 52–73% of the variance in layer LAI. Seasonal signals exhibited similar strengths over height and depth strata, and it is the well-illuminated leaf area that decreased with increasing LAI in the upper canopy, not the opposite. Therefore, a simple light limitation mechanism does not appear sufficient to explain anticorrelations between height and depth layers (evidence against H_{light}). Offering limited support for a role of direct light limitation, however, whole-canopy LAI was related positively (but nonlinearly) to incident net shortwave radiation.

The transition from the dry to the wet season was accompanied by rapid leaf area changes, with the upper canopy and understory layer both appearing to lose leaf area. The lower canopy surface, on the other hand, appears to rebound rapidly from its lowest leaf area during this seasonal transition, with new leaves potentially replacing ones already fallen. The pattern observed in the upper canopy is consistent with simultaneous abscission and new leaf emergence.

The 2015–2016 El Niño drought event had a significant impact on leaf area seasonality, strengthening seasonal patterns rather than disrupting them: seasonal changes in leaf area profiles (particularly in the lower canopy; Figs 4, S12) and leaf litterfall rates (Fig. 2b) were highest in this period (support for H_{drought}). Seasonality was variable over years (Fig. S5), and only through normalization by annual means did seasonal patterns appear regular. Reflectance seasonality metrics (EVI and NIR) were not strongly related to leaf phenological patterns (lack of support for H_{evi}).

Discussion

Leaf area phenology is vertically and environmentally structured

Our fine-scale analysis uniquely reveals height and environmental dependencies in leaf phenology that may be important to forest function, but they have been obscured in previous studies. At the plot level (250 m transects), we observed an 8.87% annual change in total LAI, which is within the range of annual changes reported from other ground-based studies of tropical evergreen forests at equivalent spatial scales (5.92–20.79%; Asner *et al.*, 2004; Doughty & Goulden, 2008; Malhado *et al.*, 2009; Brando *et al.*, 2010; Malhi *et al.*, 2014; Girardin *et al.*, 2016). At the forest level (4 km), however, the annual change was much lower (2.58%), implying that temporal patterns vary between plots, and highlighting the importance of conducting studies at larger and multiple scales. The dry season has been well documented as a period of high leaf turnover, and the wet season as a time of lower rates of leaf flush and litterfall (Goulden *et al.*, 2004; Rice *et al.*, 2004; Doughty & Goulden, 2008; Malhado *et al.*, 2009; Brando *et al.*, 2010; Albert *et al.*, 2018), as we also find here. Prior studies, however, have been limited to consideration of total LAI, which, as we show, does not represent the seasonal dynamics of the forest canopy.

Upper and lower canopy strata were highly anticorrelated within and across years (Figs 3d, S7). These findings agree with the seasonal canopy dynamics for the climate zone where the TNF is located, as documented by Tang & Dubayah (2017) with a regional timeseries of satellite LiDAR. In contrast to our monthly analysis, Tang & Dubayah (2017) included just three periods of leaf area change and considered only upper and lower leaf area compartments. Our results suggest that a higher temporal resolution can reveal key leaf area transitions – for example, between the dry and wet seasons – to better isolate roles of seasonal drought and Earth-orbital factors, such as SZA. A finer spatial resolution is also required to address height and environmental dependencies. Critically, we identified opposing seasonal and drought responses between the surface and understory layers of the lower canopy ('lower surface' and 'understory', respectively; see the Results section 'Synthesis of principal findings').

Impacts of illumination environments and height heterogeneity

What mechanisms explain the opposing synchronicity of leaf area seasonality in distinct canopy strata? One possibility is that a phenological clock determines the upper canopy pattern, whereas lower layer seasonality responds to light limitation driven by the upper canopy shifts (Tang & Dubayah, 2017). However, seasonal variation in the upper canopy opposed the lower surface, while being congruent with the understory. To explain our results in this context, the lower surface would have to be limited by lateral shading from the upper canopy, and the understory by lateral or direct (vertical) shading from the lower surface layer. However, the lower surface layer is a high light environment, whereas leaf area changes in the upper canopy are modest, such that cascading light limitation is unlikely. The approximate equivalence of relationships between distinct layers and SZA (i.e. similar correlation strengths) is also inconsistent with the upper canopy being the only stratum following a phenological clock.

Instead, tree size and functional differences may offer an alternative explanation for the opposing seasonal patterns of within-canopy layers. We identified distinct vegetation responses within three environmental zones in the canopy: the upper canopy, the lower surface, and the understory. The upper canopy likely corresponds to late successional, well-illuminated emergent and tall trees and lianas (Clark *et al.*, 2008), the lower canopy surface to light-demanding early and mid-successional trees, and the understory comprises short shade-tolerants, canopy subadults (LaFrankie *et al.*, 2006), and low branches (Stark *et al.*, 2015). Our results thus support the hypothesis that tree size and functional groups exhibit divergent phenological responses arrayed over environmental heterogeneity spanning light gaps to deep shade.

Height and canopy environments may also influence tree water status and species hydrological traits. A recent study conducted in the TNF by Brum *et al.* (2018) concluded that rooting depth, hydraulic stress resilience, and tree size all fell along a single niche axis, likely influencing the functional diversity of this seasonally dry forest. The results of our study suggest that phenological strategy may also be arrayed along this niche axis; in this case, the

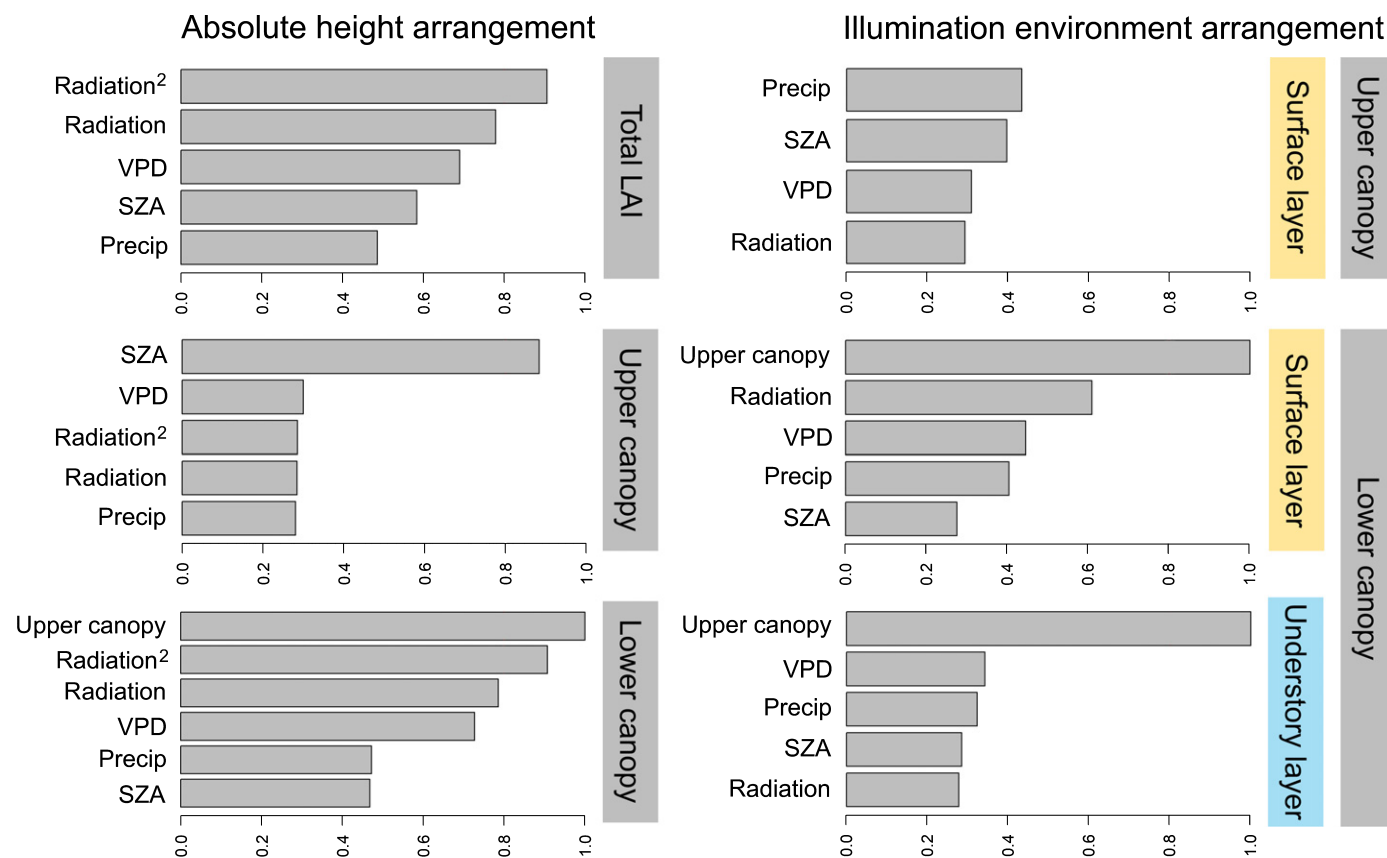


Fig. 7 Relative importance of environmental variables (vapour pressure deficit, VPD; radiation; precipitation; and solar zenith angle, SZA) in predicting seasonality of leaf area index (LAI) components for the canopy arranged by absolute height from the ground (left: total LAI, upper and lower canopy LAI) and illumination environment (distance from the local canopy surface; right: upper and lower surface LAI and understory LAI) across all possible model combinations. Models containing the best predictors were all significant except for the upper surface layer (see Supporting Information Table S3). A quadratic term for radiation was included for the analysis of the canopy data arranged by absolute height due to the presence of a significant nonlinear relationship.

combination of high light, high VPD, and low soil moisture in short-statured, shallow-rooted, canopy surface trees could lead to faster or intensified leaf abscission or reduced leaf expansion and maturation in drought, or a higher prevalence of deciduousness. The LAI increases of the understory layer suggest that smaller trees in deep shade (low illumination, low VPD) are able to tolerate, or do not experience, the same level of drought stress.

Gaps structure the vertical and horizontal heterogeneity of light environments (Chazdon & Fetcher, 1984; Denslow, 1987). The TNF has a high gap fraction (Hunter *et al.*, 2015), consistent with a high disturbance rate (Pyle *et al.*, 2008). This could explain why much of the canopy surface is low in the canopy (LAD of the surface layer peaks at 10–12 m; Fig. 5a). Thus, what may appear to be understory vegetation between 0 and 15 m in the leaf area profile (Fig. 4a) is actually predominately leaves in high illumination near the canopy surface, and this group dominates the ecosystem pattern. Future work should assess the generalisability of these findings across tropical landscapes. An important first step is to describe the landscape variation in canopy surface height distributions.

Intrinsic vs environmental controls on phenology

Is canopy phenology predominantly the result of a regular phenological clock or of environmental variability? Our study offers

strong support for a dominant phenological clock: consistent bimodal seasonality roughly corresponded with SZA (as in Borchert, 2015). We found little support for other environmental impacts in multiple regression analysis. Incident radiation and VPD were, however, important in some models and not others. By contrast, the 2015–2016 El Niño drought response offered unambiguous support for direct environmental impacts. El Niño amplified water stress (drought) over the mid to end of the dry season (Brum *et al.*, 2018), corresponding with the greatest deviation between El Niño and non-El Niño LAD profiles – layers that increased, increased slightly more; and those that decreased, decreased substantially more (Figs 4c, S12). El Niño drought intensified the phenological pattern, particularly in the water-stressed lower canopy.

Size-specific responses of trees to drought are well documented, with most studies finding increased losses of large canopy trees over a year to multiyear periods (Nepstad *et al.*, 2007; da Costa *et al.*, 2010; Phillips *et al.*, 2010). Our short-term observation of drought, in contrast, did not find negative consequences for large trees. Even at the peak of the El Niño (December 2015), large trees in the TNF were under low water stress; shallow-rooted (small) trees, by contrast, experienced exceptionally high water stress (Brum *et al.*, 2018). Accordingly, leaf area of the upper canopy remained effectively stable, but declined

considerably in the lower canopy. The work of Brum *et al.* (2018) suggests that large trees are less tolerant of water stress, operating with small safety margins, such that when deep soil water is depleted the consequences may be severe; this helps reconcile short-term resilience (deep soil water still present) with long-term large tree drought die-off. Intriguingly, Leitold *et al.* (2018) compared the TNF before and after this drought and found an intensification of canopy area loss (from the canopy surface) and coarse woody debris production. Since they surveyed with LiDAR 3 months after the measurements made by Brum *et al.* (2018), their study may capture delayed drought-induced tree or branch die-back. Liu *et al.* (2018) also found satellite-based reflectance consistent with an initial increase in canopy growth at the onset of drought and subsequent canopy senescence.

Implications for satellite remote sensing and modelling forest productivity

Recent research has found that leaf demography plays an important role in determining seasonal change in whole-canopy function. The fractions of different leaf age classes appear to strongly influence canopy radiation environments and reflectance, and canopy production capacity (Wu *et al.*, 2016, 2018; Albert *et al.*, 2018). Our results suggest that contrasting phenological processes may cause age class proportions to vary over canopy heights and environments, influencing emergent NIR reflectance and EVI patterns, and potentially GPP seasonality. This dynamically structured leaf demography is indicated by the distinct timings and directions of large shifts in leaf area in different canopy environments.

With regard to satellite reflectance, the hypothesis that the decomposition of LAI into height- and environment-stratified components could predict EVI was not supported (see Table S2). Our analyses instead support previous findings that leaf age and function are stronger determinants of EVI than leaf quantity (Wu *et al.*, 2018). However, the interpretation of whole-canopy reflectance could be refined by accounting for the abundance distribution of distinct canopy strata in a forest, and their associated unique phenologies and sensitivities to drought. Our observations of LAI shifts are composites of leaf flush and leaf fall, and therefore cannot distinguish leaf demography. But our study provides a template for future work to explore the vertical structuring of leaf demography and test its relationship to satellite derived reflectance indices.

Vegetation models that integrate non-height-structured sun and shaded leaf fractions (de Pury & Farquhar, 1997) will be unlikely to capture the divergent phenological and drought responses of sun leaves in the upper vs lower canopy levels that we observed. How those divergent responses translate to leaf function and how that, in turn, scales to whole forest function remains uncertain. In addition, our work motivates an exploration of the impact of incorporating height and environmentally resolved leaf demographic patterns into models (Fisher *et al.*, 2018). Empirical work to characterise leaf demography and leaf function through the vertical canopy and across light environments will be critical to this effort. Incorporating these factors

may improve model predictions of forest–atmosphere exchanges in the Amazon.

Conclusions

Leaf phenology and responses to an exceptional drought in an eastern Amazonian forest were structured by canopy height and leaf environment. Short trees at the canopy surface displayed strong contrasting patterns with respect to other vegetation. Leaf area decreased in low canopy surfaces over the dry season, a pattern that may be attributable to a combination of high leaf stress and low soil water availability. Phenology was characteristically bimodal following roughly SZA dynamics, suggesting a phenological clock mechanism, even while the dry- to wet-season transition was characterised by rapid dynamics. Modest leaf area changes may obscure larger changes in leaf age and functional composition, and future empirical and modelling efforts can improve understanding of canopy function by accounting for height- and environment-dependent phenology. These advances are crucial for understanding responses to increasing droughts under climate change; if tree phenological and hydrological strategies are linked, as our research suggests, this could determine the species that are winners and losers under shifting drought regimes in tropical forests. This study also offers a clear demonstration of the utility of LiDAR for estimating fine-scale canopy structure to better understand changing forest phylloenvironments and their consequences.

Acknowledgements









Special thanks to Cleuton Pereira and Francisco Alves de Freitas Neto ('Chico') for their help with data collection, to GOAmazon co-PI Marciel Ferreira for collaboration, and to the Large-Scale Biosphere–Atmosphere Experiment in Amazonia project for field infrastructure and support. This work was supported by the National Science Foundation's (NSF's) Partnerships for International Research and Education (#OISE-0730305) and the GOAmazon project (award #3002937712), funded jointly by the US Department of Energy and the Brazilian state science foundations in São Paulo and Amazonas (FAPESP/FAPEAM # 2013/50533-5). Financial support was provided to MNS by the National Aeronautics and Space Administration (NASA) (NESS-F-NNX14AK95H), to SCS by NSF (EF-1550686 and EF-1340-604) and NASA (award #NNX17AF65G), to TCT by NSF (PRFB-1711997), and to SMM by NSF (EF-1137366 and EF-1638490).

Author contributions

MNS, SCS, and SRS conceived the study, designed the analyses, and led the data interpretation, with extensive help from TEH, TCT, SMM, and DAF. MNS performed the data analysis and drafted the manuscript, with substantial input from SCS, SRS, TEH, TCT, SMM, and DAF. MLF, EdO, LFA, MF, PBdC, and RCdO collected or managed leaf litterfall collections. MNS, DBdS, TW, SCS, and RCdO collected or managed LiDAR

measurements. NRC, RCdO, PBdC, LEOCA, and SRS contributed to the installation, maintenance, or analysis of environmental data from the K67 flux tower, and NRC provided TRMM data. SC provided EVI and NIR data. SCS wrote the core functions to process the LiDAR data and the resampling scheme. All authors contributed towards writing the final manuscript.

ORCID

Luciana F. Alves  <https://orcid.org/0000-0002-8944-1851>
Raimundo C. de Oliveira  <https://orcid.org/0000-0002-2735-1746>
Donald A. Falk  <https://orcid.org/0000-0003-3873-722X>
Mauricio L. Ferreira  <https://orcid.org/0000-0002-7647-3635>
Sean M. McMahon  <https://orcid.org/0000-0001-8302-6908>
Natalia Restrepo-Coupe  <https://orcid.org/0000-0003-3921-1772>
Marielle N. Smith  <https://orcid.org/0000-0003-2323-331X>
Tyen C. Taylor  <https://orcid.org/0000-0002-0926-098X>

References

- Albert LP, Wu J, Prohaska N, De Camargo PB, Huxman TE, Tribuzy ES, Ivanov VY, Oliveira RS, Garcia S, Smith MN *et al.* 2018. Age-dependent leaf physiology and consequences for crown-scale carbon uptake during the dry season in an Amazon evergreen forest. *New Phytologist* 219: 870–884.
- Asner GP, Nepstad D, Cardinot G, Ray D. 2004. Drought stress and carbon uptake in an Amazon forest measured with spaceborne imaging spectroscopy. *Proceedings of the National Academy of Sciences, USA* 101: 6039–6044.
- Biudes MS, Machado NG, de Moraes Danelichen VH, Souza MC, Vourlitis GL, de Souza Nogueira J. 2014. Ground and remote sensing-based measurements of leaf area index in a transitional forest and seasonal flooded forest in Brazil. *International Journal of Biometeorology* 58: 1181–1193.
- Borchert R. 1980. Phenology and ecophysiology of tropical trees: *Erythrina poeppigiana*. *Ecology* 61: 1065–1074.
- Borchert R. 2015. Insolation and photoperiodic control of tree development near the equator. *New Phytologist* 205: 7–13.
- Bradley AV, Gerard FF, Barbier N, Weedon GP, Anderson LO, Huntingford C, Aragão LEOC, Zelazowski P, Arai E. 2011. Relationships between phenology, radiation and precipitation in the Amazon region. *Global Change Biology* 17: 2245–2260.
- Brando PM, Goetz SJ, Baccini A, Nepstad DC, Beck PSA, Christman MC. 2010. Seasonal and interannual variability of climate and vegetation indices across the Amazon. *Proceedings of the National Academy of Sciences, USA* 107: 14685–14690.
- Brum M, Vadeboncoeur MA, Ivanov V, Saleska S, Alves LF, Penha D, Asbjornsen H, Dias JD, Aragão LEOC, Barros F *et al.* 2018. Hydrological niche segregation defines forest structure and drought tolerance strategies in a seasonal Amazon forest. *Journal of Ecology* 107: 318–333.
- Calcagno V, da Mazancourt C. 2010. GLMULTI: an R package for easy automated model selection with (generalized) linear models. *Journal of Statistical Software* 34: 1–29.
- Chadwick R, Good P, Martin G, Rowell DP. 2015. Large rainfall changes consistently projected over substantial areas of tropical land. *Nature Climate Change* 6: 177–182.
- Chazdon RL, Fetcher N. 1984. Photosynthetic light environments in a lowland tropical rain forest in Costa Rica. *Journal of Ecology* 72: 553–564.
- Clark DB, Olivas PC, Oberbauer SF, Clark DA, Ryan MG. 2008. First direct landscape-scale measurement of tropical rain forest leaf area index, a key driver of global primary productivity. *Ecology Letters* 11: 163–172.
- da Costa ACL, Galbraith D, Almeida S, Portela BTT, da Costa M, Silva Junior JDA, Braga AP, de Gonçalves PHL, de Oliveira AAR, Fisher R *et al.* 2010. Effect of 7 yr of experimental drought on vegetation dynamics and biomass storage of an eastern Amazonian rainforest. *New Phytologist* 187: 579–591.
- Denslow J. 1987. Tropical rainforest gaps and tree species diversity. *Annual Review of Ecology, Evolution, and Systematics* 18: 431–451.
- Dirzo R, Raven PH. 2003. Global state of biodiversity and loss. *Annual Review of Environment and Resources* 28: 137–167.
- Domingues TF, Berry JA, Martinelli LA, Ometto JPHB, Ehleringer JR. 2005. Parameterization of canopy structure and leaf-level gas exchange for an eastern Amazonian tropical rain forest (Tapajós National Forest, Pará, Brazil). *Earth Interactions* 9: 1–23.
- Doughty C, Goulden M. 2008. Seasonal patterns of tropical forest leaf area index and CO₂ exchange. *Journal of Geophysical Research* 113: 1–12.
- Duffy PB, Brando P, Asner GP, Field CB. 2015. Projections of future meteorological drought and wet periods in the Amazon. *Proceedings of the National Academy of Sciences, USA* 112: 13172–13177.
- Fisher RA, Christoffersen O, Longo M, Viskari T, Koven CD, Anderegg WRL, Dietze MC, Farrior CE, Holm JA, Hurtt GC *et al.* 2018. Vegetation demographics in Earth system models: a review of progress and priorities. *Global Change Biology* 24: 35–54.
- Garcia ES, Swann ALS, Villegas JC, Breshears DD, Law DJ, Saleska SR, Stark SC. 2016. Synergistic ecoclimate teleconnections from forest loss in different regions structure global ecological responses. *PLoS ONE* 11: e165042.
- Gedney N, Valdes P. 2000. The effect of Amazonian deforestation on the Northern Hemisphere circulation and climate. *Geophysical Research Letters* 27: 3053–3056.
- Girardin CAJ, Malhi Y, Doughty CE, Metcalfe DB, Meir P, Aguila-Pasquel J, Araujo-Murakami A, Costa ACL, Silva-Espejo JE, Amézquita FF *et al.* 2016. Seasonal trends of Amazonian rainforest phenology, net primary productivity, and carbon allocation. *Global Biogeochemical Cycles* 30: 700–715.
- Goulden M, Miller S, da Rocha HR, Menton M, de Freitas H, e Silva Figueira AM, de Souza CA. 2004. Diel and seasonal patterns of tropical forest CO₂ exchange. *Ecological Applications* 14: 42–54.
- Guan K, Pan M, Li H, Wolf A, Wu J, Medvigy D, Caylor KK, She J, Wood EF, Malhi Y *et al.* 2015. Photosynthetic seasonality of global tropical forests constrained by hydroclimate. *Nature Geoscience* 8: 284–289.
- Huete AR, Didan K, Shimabukuro YE, Ratana P, Saleska SR, Hutyrá LR, Yang W, Nemani RR, Myneni R. 2006. Amazon rainforests green-up with sunlight in dry season. *Geophysical Research Letters* 33: L06405.
- Hunter MO, Keller M, Morton D, Cook B, Lefsky M, Ducey M, Saleska S, de Oliveira RC, Schietti J. 2015. Structural dynamics of tropical moist forest gaps. *PLoS ONE* 10: e0132144.
- Hutyrá LR, Munger JW, Saleska SR, Gottlieb E, Daube BC, Dunn AL, Amaral DF, de Camargo PB, Wofsy SC. 2007. Seasonal controls on the exchange of carbon and water in an Amazonian rain forest. *Journal of Geophysical Research* 112: G03008.
- LaFrankie JV, Ashton PS, Chuyong GB, Co L, Davies SJ, Foster R, Hubbell SP, Kenfack D, Losos EC, Nor NS *et al.* 2006. Contrasting structure and composition of the understory in species-rich tropical rain forests. *Ecology* 87: 2298–2305.
- Leitold V, Morton DC, Longo M, Dos-Santos MN, Keller M, Scaranello M. 2018. El Niño drought increased canopy turnover in Amazon forests. *New Phytologist* 219: 959–971.
- Liu YY, Van Dijk AIJM, Miralles DG, McCabe MF, Evans JP, De Jeu RAM, Gentile P, Huete A, Parinussa RM, Wang L *et al.* 2018. Enhanced canopy growth precedes senescence in 2005 and 2010 Amazonian droughts. *Remote Sensing of Environment* 211: 26–37.
- Lyapustin AI, Wang Y, Laszlo I, Hilker T, Hall FG, Sellers PJ, Tucker CJ, Korkin SV. 2012. Multi-angle implementation of atmospheric correction for MODIS (MAIAC): 3. Atmospheric correction. *Remote Sensing of Environment* 127: 385–393.
- MacArthur R, Horn H. 1969. Foliage profile by vertical measurements. *Ecology* 50: 802–804.
- Malhado ACM, Costa MH, de Lima FZ, Portillo KC, Figueiredo DN. 2009. Seasonal leaf dynamics in an Amazonian tropical forest. *Forest Ecology and Management* 258: 1161–1165.

- Malhi Y, Aragão LEOC, Galbraith D, Huntingford C, Fisher R, Zelazowski P, Sitch S, McSweeney C, Meir P. 2009. Exploring the likelihood and mechanism of a climate-change-induced dieback of the Amazon rainforest. *Proceedings of the National Academy of Sciences, USA* 106: 20610–20615.
- Malhi Y, Farfán Amézquita F, Doughty CE, Silva-Espejo JE, Girardin CAJ, Metcalfe DB, Aragão LEOC, Huaraca-Quispe LP, Alzamora-Taype I, Eguiluz-Mora L *et al.* 2014. The productivity, metabolism and carbon cycle of two lowland tropical forest plots in south-western Amazonia, Peru. *Plant Ecology & Diversity* 7: 85–105.
- Malhi Y, Roberts JT, Betts RA, Killeen TJ, Li W, Nobre CA. 2008. Climate change, deforestation, and the fate of the Amazon. *Science* 319: 169–172.
- Morton DC, Nagol J, Carabahal CC, Rosette J, Palace M, Cook BD, Vermote EF, Harding DJ, North PRJ. 2014. Amazon forests maintain consistent canopy structure and greenness during the dry season. *Nature* 506: 221–224.
- Nepstad DC, Tohver IM, Ray D, Moutinho P, Cardinot G. 2007. Mortality of large trees and lianas following experimental drought in an Amazon forest. *Ecology* 88: 2259–2269.
- NOAA ESRL Global Monitoring Division. 2018. *NOAA solar calculator*. Boulder, CO, USA. [WWW document] URL <http://esrl.noaa.gov/gmd/grad/solcalc/> [accessed 4 June 2018].
- Pan Y, Birdsey Ra, Fang J, Houghton R, Kauppi PE, Kurz Wa, Phillips OL, Shvidenko A, Lewis SL, Canadell JG *et al.* 2011. A large and persistent carbon sink in the world's forests. *Science* 333: 988–993.
- Parker GG, Harding DJ, Berger ML. 2004. A portable LiDAR system for rapid determination of forest canopy structure. *Journal of Applied Ecology* 41: 755–767.
- Phillips OL, Van Der Heijden G, Lewis SL, López-González G, Aragão LEOC, Lloyd J, Malhi Y, Monteagudo A, Almeida S, Dávila EA *et al.* 2010. Drought–mortality relationships for tropical forests. *New Phytologist* 187: 631–646.
- de Pury DGG, Farquhar GD. 1997. Simple scaling of photosynthesis from leaves to canopies without the errors of big-leaf models. *Plant, Cell & Environment* 20: 537–557.
- Pyle EH, Santoni GW, Nascimento HEM, Hutrya LR, Vieira S, Curran DJ, van Haren J, Saleska SR, Chow VY, Carmago PB *et al.* 2008. Dynamics of carbon, biomass, and structure in two Amazonian forests. *Journal of Geophysical Research* 113: G00B08.
- R Core Team. 2016. *R: a language and environment for statistical computing*. R v.3.5.1. Vienna, Austria: R Foundation for Statistical Computing. [WWW document] URL <https://www.R-project.org/> [accessed 3 August 2018].
- Reich P. 1995. Phenology of tropical forests: patterns, causes, and consequences. *Canadian Journal of Botany* 174: 164–174.
- Restrepo-Coupe N, da Rocha HR, Hutrya LR, da Araujo AC, Borma LS, Christoffersen B, Cabral OMR, de Camargo PB, Cardoso FL, da Costa ACL *et al.* 2013. What drives the seasonality of photosynthesis across the Amazon basin? A cross-site analysis of eddy flux tower measurements from the Brasil flux network. *Agricultural and Forest Meteorology* 182–183: 128–144.
- Restrepo-Coupe N, Levine NM, Christoffersen BO, Albert LP, Wu J, Costa MH, Galbraith D, Imbuzeiro H, Martins G, da Araujo AC *et al.* 2017. Do dynamic global vegetation models capture the seasonality of carbon fluxes in the Amazon basin? A data-model intercomparison. *Global Change Biology* 23: 191–208.
- Rice AH, Pyle EH, Saleska SR, Hutrya L, Michael P, Keller M, de Camargo PB, Portillo K, Marques DF, Wofsy SC. 2004. Carbon balance and vegetation dynamics in an old-growth Amazonian forest. *Ecological Applications* 14: S55–S71.
- Rivera G, Elliott S, Caldas LS, Nicolossi G, Coradin VT, Borchert R. 2002. Increasing day-length induces spring flushing of tropical dry forest trees in the absence of rain. *Trees* 16: 445–456.
- Saleska SR, Didan K, Huete AR, da Rocha HR. 2007. Amazon forests green-up during 2005 drought. *Science* 318: 612.
- Saleska SR, Miller SD, Matross DM, Goulden ML, Wofsy SC, da Rocha HR, de Camargo PB, Crill P, Daube BC, de Freitas HC *et al.* 2003. Carbon in Amazon forests: unexpected seasonal fluxes and disturbance-induced losses. *Science* 302: 1554–1557.
- Saleska SR, Wu J, Guan K, Araujo AC, Huete A, Nobre AD, Restrepo-Coupe N. 2016. Dry-season greening of Amazon forests. *Nature* 531: E4–E5.
- van Schaik C, Terborgh J, Wright S. 1993. The phenology of tropical forests: adaptive significance and consequences for primary consumers. *Annual Review of Ecology and Systematics* 24: 353–377.
- Sitch S, Huntingford C, Gedney N, Levy PE, Lomas M, Piao SL, Betts R, Ciais P, Cox P, Friedlingstein P *et al.* 2008. Evaluation of the terrestrial carbon cycle, future plant geography and climate–carbon cycle feedbacks using five dynamic global vegetation models (DGVMs). *Global Change Biology* 14: 2015–2039.
- Smith AP, Hogan KP, Idol JR. 1992. Spatial and temporal patterns of light and canopy structure in a lowland tropical moist forest. *Biotropica* 24: 503–511.
- Spracklen DV, Arnold SR, Taylor CM. 2012. Observations of increased tropical rainfall preceded by air passage over forests. *Nature* 489: 282–285.
- Stark SC, Enquist BJ, Saleska SR, Leitold V, Schiatti J, Longo M, Alves LF, Camargo PB, de Oliveira RC. 2015. Linking canopy leaf area and light environments with tree size distributions to explain Amazon forest demography. *Ecology Letters* 18: 636–645.
- Stark SC, Leitold V, Wu JL, Hunter MO, de Castilho CV, Costa FRC, McMahon SM, Parker GG, Shimabukuro MT, Lefsky MA *et al.* 2012. Amazon forest carbon dynamics predicted by profiles of canopy leaf area and light environment. *Ecology Letters* 15: 1406–1414.
- Tang H, Dubayah R. 2017. Light-driven growth in Amazon evergreen forests explained by seasonal variations of vertical canopy structure. *Proceedings of the National Academy of Sciences, USA* 114: 2640–2644.
- Time and Date AS. 2018. [WWW document] URL <https://www.timeanddate.com/sun/brazil/santarem> [accessed 26 January 2018].
- Tropical Rainfall Measuring Mission (TRMM). 2011. *TRMM (TMPA/3B43) rainfall estimate L3 1 month 0.25 degree × 0.25 degree V7*. Greenbelt, MD, USA: Goddard Earth Sciences Data and Information Services Center. [WWW document] URL https://disc.gsfc.nasa.gov/datacollection/TRMM_3B43_7.html [accessed 24 March 2017].
- Wagner FH, Hérault B, Rossi V, Hilker T, Maeda EE, Sanchez A, Lyapustin AI, Galvão LS, Wang Y, Aragão LEOC. 2017. Climate drivers of the Amazon forest greening. *PLoS ONE* 12: e0180932.
- Werth D, Avissar R. 2002. The local and global effects of Amazon deforestation. *Journal of Geophysical Research* 107: 8087.
- Wright S, van Schaik C. 1994. Light and the phenology of tropical trees. *American Naturalist* 143: 192–199.
- Wright SJ, Kitajima K, Kraft NJB, Reich PB, Ian J, Bunker DE, Condit R, Dalling JW, Davies SJ, Díaz S *et al.* 2010. Functional traits and the growth–mortality trade-off in tropical trees. *Ecology* 91: 3664–3674.
- Wu J, Albert LP, Lopes AP, Restrepo-Coupe N, Hayek M, Wiedemann KT, Guan K, Stark SC, Christoffersen B, Prohaska N *et al.* 2016. Leaf development and demography explain photosynthetic seasonality in Amazon evergreen forests. *Science* 351: 972–976.
- Wu J, Kobayashi H, Stark SC, Meng R, Guan K, Tran NN, Gao S, Yang W, Restrepo-coupe N, Miura T *et al.* 2018. Biological processes dominate seasonality of remotely sensed canopy greenness in an Amazon evergreen forest. *New Phytologist* 217: 1507–1520.

Supporting Information

Additional Supporting Information may be found online in the Supporting Information section at the end of the article.

Fig. S1 Leaf area density profiles for lidar instrument intercomparison.

Fig. S2 LAI layer timeseries to assess resampling based approach testing for artefactual profile changes.

Fig. S3 Seasonal leaf area profile changes to assess resampling based approach testing for artefactual profile changes.

Fig. S4 Measurement error derived from repeat measurements compared against seasonal profile changes.

Fig. S5 Normalised and absolute values of total, upper, and lower LAI for each survey year.

Fig. S6 Timeseries of LAI, dLAI, and leaf litterfall used to generate leaf flush estimates.

Fig. S7 Linear regressions between lower and upper canopy LAI for each survey year.

Fig. S8 Plot-level seasonal dynamics for total, upper, and lower LAI during the El Niño year.

Fig. S9 Seasonal changes in leaf area density profiles for each survey year.

Fig. S10 Seasonal changes in leaf area profiles separated into canopy depth layers for non-El Niño and El Niño years.

Fig. S11 Linear regressions between highly correlated LAI layers for the illumination environment canopy arrangement.

Fig. S12 Seasonal changes in leaf area profiles highlighting non-El Niño vs El Niño changes for each canopy depth layer.

Fig. S13 Quadratic relationships between LAI layers and daylength and radiation.

Notes S1 Lidar data collections and instrument intercomparison.

Notes S2 Testing for sampling sensitivities and potential lidar methodological artefacts.

Notes S3 Quantifying lidar measurement error.

Notes S4 K67 seasonal leaf area profile data.

Notes S5 Results of multiple regression analysis including daylength as the phenological variable.

Table S1 Means, ranges, and normalised ranges, of leaf flush, litterfall, and LAI layers.

Table S2 Analysis of correlations between canopy LAI layers, orbitally determined environmental variables, and EVI and NIR reflectance.

Table S3 Best linear regression models of LAI layers predicted from environmental variables, including SZA.

Table S4 Best linear regression models of LAI layers predicted from environmental variables, including daylength.

Please note: Wiley Blackwell are not responsible for the content or functionality of any Supporting Information supplied by the authors. Any queries (other than missing material) should be directed to the *New Phytologist* Central Office.